Damping of acoustic vibrations of single gold nanoparticles optically trapped in water: Supporting Information

P. V. Ruijgrok,[1] P. Zijlstra,[1] A. L. Tchebotareva [1] and M. Orrit[1]

[1] Institute of Physics, Leiden University, P.O. Box 9504, 2300 RA Leiden, The Netherlands

Particle temperature in the optical trap

Here we estimate the temperature of the gold nanoparticles in the optical trap, due to absorption of the trapping laser.

We calculate the particle temperature as

$$\Delta T = \frac{P_{\mathrm{abs}}}{4\pi\kappa R} = \frac{\sigma_{\mathrm{abs}} I}{4\pi\kappa R} \tag{1}$$

where κ is the thermal conductivity of water, R is the particle radius, σ_{abs} is the absorption cross section of the nanoparticle at the wavelength of the trapping laser, and I is the intensity of the trap laser at the focal plane.

We estimate the intensity at the trap focus I_{fp} from the optical power in the focal plane P_{fp} as

$$I_{\mathrm{fp}} = \frac{2\pi P_{\mathrm{fp}} \mathrm{NA}^2}{\lambda^2} \tag{2}$$

where NA is the numerical aperture and λ is the wavelength of the trap laser. We take an effective numerical aperture NA of 1.0, as characterized previously for our trapping geometry in experiments on gold nanorods [1]. We take the effective intensity at the trap focus to be half the value predicted by eq 2, due to aberrations resulting from the relative large trapping depth, as found previously for our setup with trapping depths about 25 μm away from the glass substrate [1]. We neglect intensity changes resulting from a displacement from the focus. We also account for the measured objective transmission of 19 % at the trap wavelength to compute the power at the focal plane from the power measured at the back focal plane of the objective. We find for a power of 75 mW at the focus (the highest trapping power used) an effective intensity of 2.0×10^{11} W/m^2.

We calculated the absorption cross section of the 80 nm spheres using Mie theory. For the rods (about 25 nm diameter and 60 nm length), the absorption cross section was calculated in the electrostatic approximation for an ellipsoid, see Table S 1.

For the highest trapping power of 75 mW used in the experiment, we find a temperature increase of about 60 K for a 80 nm diameter gold particle, and about 80 K for a gold nanorod, see Table S 2.

Particle	Wavelength	σ_{abs} (m^2)	σ_{sca} (m^2)
Sphere	$\lambda_{\mathrm{res,abs}}$ (540 nm)	$1.9\,10^{-14}$	–
	$\lambda_{\mathrm{res,sca}}$ (560 nm)	–	$1.5\,10^{-14}$
	λ_{probe} (590 nm)	$7.1\,10^{-15}$	$1.0\,10^{-14}$
	λ_{pump} (785 nm)	$2.7\,10^{-16}$	$9.5\,10^{-16}$
	λ_{trap} (1064 nm)	$9.5\,10^{-17}$	$1.9\,10^{-16}$
Rod	$\lambda_{\mathrm{res,abs}}$ (623 nm)	$2.0\,10^{-14}$	–
	$\lambda_{\mathrm{res,sca}}$ (626 nm)	–	$3.8\,10^{-15}$
	λ_{probe} (610 nm)	$1.5\,10^{-14}$	$2.5\,10^{-15}$
	λ_{pump} (785 nm)	$3.3\,10^{-16}$	$9.5\,10^{-17}$
	λ_{trap} (1064 nm)	$6.3\,10^{-17}$	$1.2\,10^{-17}$

Table S1 Calculated absorption cross-sections σ_{abs} and scattering cross-sections σ_{sca} for a gold nanosphere and a gold nanorod, of typical dimensions used in our experiment. The cross sections are tabulated at the wavelengths of the plasmon resonance (λ_{res}), probe beam (λ_{probe}), pump beam (λ_{pump}) and trapping beam (λ_{trap}). The refractive index of the environment of the particles was that of water (n = 1.33). The optical constants of gold were taken from from Johnson and Christy. [2]. For the sphere (80 nm diameter), cross-sections were calculated using Mie theory [3]. The cross-sections for the nanorod were calculated in the electrostatic approximation for an ellipsoid, for a polarization parallel to the long axis of the rod. We take into account corrections for radiation damping and electron surface scattering [4], as reported previously [1]. The tabulated values for the nanorod are chosen for a nanorod with an aspect ratio of 2.4, and a volume of $2.5\,10^{-24}$ m^3, equal to the ensemble-averaged volume of the rods determined from electron microscopy on the sample.

Particle	ΔT (K/mW)	$\Delta T\|_{75\,\mathrm{mW}}$ (K)
Sphere	0.8 ± 0.3	60 ± 30
Rod	1.1 ± 0.3	85 ± 30

Table S2 Calculated temperature increase ΔT of spheres and rods in the optical trap in water, due to absorption of the trapping laser at 1064 nm. Values are calculated for a gold nanosphere (80 nm diameter) and a nanorod (about 25 nm diameter, 60 nm length) using Eq. 1 with absorption cross sections from Table S 1, intensity $I = 2.0 \times 10^{11}\,\mathrm{W/m^2}$ for 75 mW power at the focal plane and thermal conductivity $\kappa = 0.65\,\mathrm{W\,m^{-1}\,K^{-1}}$. The temperature increase of the rod was calculated using Eq. 1 with the radius of a sphere of the same volume as the rod.

Particle temperature after pulsed excitation

Here we estimate the particle lattice temperature increase due to pump and probe laser pulses.

The energy E_{abs} absorbed by the nanoparticle from a pulse with energy E_{pulse} can be approximated as

$$E_{\mathrm{abs}} = \frac{\sigma_{\mathrm{abs}}}{A} E_{\mathrm{pulse}} \tag{3}$$

where σ_{abs} is the absorption cross section of the nanoparticle at the wavelength of the pulsed laser and A is the cross-sectional area at the focus of the pulsed laser beam. The cross-sectional areas of the pump and probe beams are not measured independently in our experiment. To obtain an upper limit on the absorbed energy, we assume a diffraction limited spot with effective NA 1.0, as found previously [1] for the trap laser in our experimental setup. For the pump ($\lambda = 785\,\mathrm{nm}$) and probe ($\lambda = 590\,\mathrm{nm}$) beams we then find cross-sectional areas of at least $1.8\,10^{-13}\,\mathrm{m}^2$ and $1.0\,10^{-13}\,\mathrm{m}^2$.

The initial temperature increase of the the lattice can be calculated from the absorbed energy as

$$\Delta T|_{t=0} = \frac{E_{abs}}{C_p V_p} \tag{4}$$

where C_p is the heat capacity of the solid gold ($24.9\,10^5\,\mathrm{J\,K^{-1}\,m^{-3}}$) and V_p is the particle volume ($2.68\,10^{-22}\,\mathrm{m}^3$ for spheres and $2.5\,10^{-23}\,\mathrm{m}^3$ for rods).

For the typical pump and probe beam energies and wavelengths used, we find upper limits of the transient lattice temperature rise of about 20 K for the nanospheres, and about 300-400 K for the rods. See table S 3. The temperature rises of the nanoparticles in our experiment are expected to be below these values.

Particularly for the nanorods, the estimated lattice temperatures are appreciable, and we may worry about thermally induced shape changes of the rod. Thermally induced reshaping however, it mostly determined by the average temperature rise, as long as the temperature is below the melting point of the rods. Reshaping of the rods is initiated by thermal diffusion of surface atoms, that tends to drive the rod towards the thermodynamically more favorable spherical shape [5]. For the nanorods in water, the pump-probe induced lattice temperature rise decays with a characteristic time around of 100 ps, about 100 times shorter than the time in between pulses (13 ns). Due to this low duty cycle the time-averaged temperature increase of the nanorods is still small (< 1 K), and no reshaping is expected. This is in agreement with ultrafast studies on ensembles of gold nanorods, where no structural reshaping was observed for transient lattice temperatures below 700 °C. The melting of gold nanorods upon absorption of ultrafast laser pulses has also been measured on single gold nanorods [6]. It was found that gold nanorods of 30 nm diameter and 90 nm length melted only when lattice temperatures reached values around the melting temperature of bulk gold at 1330 K. Most importantly, we can confirm that the rods have not reshaped in our experiment by a measurement of the scattering spectrum of the rods before and after excitation with laser pulses, where reshaping would be seen by changes of the longitudinal plasmon resonance. See Fig. S 1 below and the accompanying text.

Particle	Beam	E_{pulse} (pJ)	E_{abs} (fJ)	$\Delta T\|_{t=0}$ (K)
Sphere	Pump (λ_{pump} (785 nm)	10 ± 3	15 ± 5	22 ± 7
	Probe (λ_{probe} (590 nm)	0.20 ± 0.05	9.0 ± 2.3	20 ± 7
Rod	Pump (λ_{pump} (785 nm)	10 ± 3	18 ± 6	290 ± 100
	Probe (λ_{probe} (610 nm)	0.20 ± 0.05	28.0 ± 10	450 ± 150

Table S3 Calculated upper bounds for the transient lattice temperature increase ΔT immediately after the absorption of pump and probe pulses, for gold nanospheres (80 nm diameter) and nanorods (25 nm diameter, 60 nm length). The energy E_{abs} absorbed by the particle due to the pump or probe pulsed is calculated from the pulse energy E_{pulse} using Eq. 3, with the absorption cross section from Table S 1.

Scattering spectra of single trapped nanorods

For all gold nanorods on which we have recorded a vibrational trace, we have recorded white-light scattering spectra to confirm that a single gold nanorod is trapped. An example of such a spectrum is shown in Figure S 1, together with an indication of the wavelengths of the pump and probe pulses that were used for this rod. The spectrum is well fitted by a Lorentzian (in energy), with a resonance at $\lambda_L = 645\,\text{nm}$ and a FWHM of 50 nm (150 meV). The symmetric shape of the spectrum and its narrow linewidth show that only a single nanorod is trapped [1]. The wavelength of the resonance is directly related to the aspect ratio of the nanorod. In our experiment we measure rods with resonance wavelengths from 590 nm to about 650 nm, around the ensemble-averaged value of 627 nm (measured independently in a UV-VIS photospectrometer). These plasmon resonance wavelengths are in good agreement with the expected values for gold nanorods of aspect ratio around 2.5, in water.

We have also measured scattering spectra of individual gold nanorods before and after the pump-probe measurement, to check for reshaping of the rod. Here, reshaping of the nanorods would be observable as a blue-shift of the plasmon resonance. The extreme case of complete melting of the rod would be easily observable by a shift of the resonance to around 530 nm. For some nanorods, in particular the rods with longer resonance wavelengths (larger aspect ratios) blue shifts of up to 20 nm were observed. For most nanorods, no large blue-shifts larger than 2-3 nm were detected over the course of a pump-probe measurement, about 5-10 minutes. These plasmon shifts are comparable to the shifts induced by the slow reshaping of the rod in the optical trap. This slow reshaping occurs even the in absence of the pump-probe pulses [1]. The stability of the plasmon resonance shows that the rods did not significantly reshape due to the absorption of the pump and probe pulses.

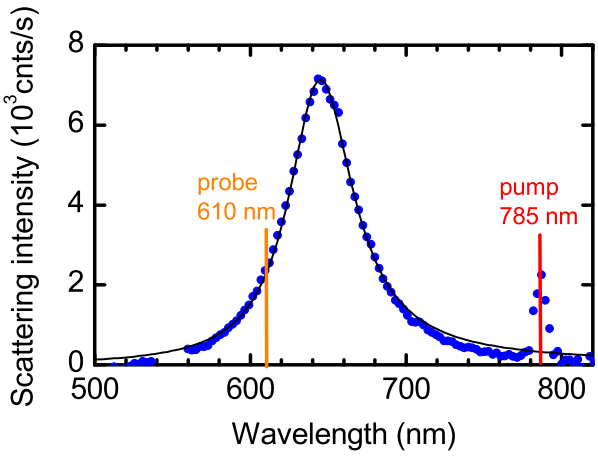

Figure S1 White light scattering spectrum for a single gold nanorod trapped in water. This spectrum was measured on the rod for which the vibrational trace is presented in Fig 3(a) of the main text. The solid line is a Lorentzian fit (in energy) of the data, with a resonance at $\lambda_\text{L} = 645\,\text{nm}$ and a full width at half maximum 50 nm. The small peak observed at 785 nm is due to residual pump light.

Vibrational modes of gold nanospheres

In our experiment, the vibrational response of the trapped gold nanospheres is dominated by the breathing mode. However, weak signatures of other vibration modes are detected on some particles. The vibration modes of an elastic sphere have been first calculated by Lamb more than a century ago [7]. The vibration modes in Lamb's theory are labeled by two integers, n, the harmonic order, i.e. the number of radial nodes, and l, the angular momentum number, representing the angular dependence of the mode.

Fig. S 2 (a) shows a vibrational spectrum of a trapped sphere that displayed several vibration frequencies. Besides the fundamental breathing mode $(n, l) = (0, 0)$ at $\Omega_{0,0} = 38.8\,\mathrm{GHz}$, vibration modes are detected at 84 GHz and 126 GHz. These frequencies are close to the values calculated in Lamb's theory for the first higher order radial modes of a 80 nm gold sphere [8] with a free boundary condition, taking the bulk elastic constants of gold. For the first higher order radial modes $(1, 0)$ and $(2, 0)$ the calculated frequencies are $\Omega_{1,0} = 2.10\,\Omega_{0,0}$ and $\Omega_{2,0} = 3.18\,\Omega_{0,0}$. The $(1, 0)$ radial mode was detected for 3 out of the 10 investigated single gold spheres. The excitation and detection of this mode appears robust: if the mode was found for a particular sphere, it was observed in each of several (2-5) consecutive vibrational spectra acquired on that particle in the optical trap, over a time span of up to 30 minutes. The second order radial mode $(2, 0)$ was clearly observed for 2 out the 3 the particles that displayed the $(1, 0)$ mode, but in both cases appeared in only one trace out of a series of vibrational traces acquired on the particle.

Some particles (3 out of 10) displayed a weak vibration mode with a frequency around 0.3 times the breathing mode frequency. A vibrational spectrum of a such a particle is shown in Fig. S 2 (b). The mode at 12.5 GHz is possibly the non-spherically symmetric $(n, l) = (0, 2)$ mode, corresponding to a uniaxial cigar-to-pancake deformation of the spheres. The excitation of this mode is not expected for spheres, embedded in an isotropic environment and subject to a spherically symmetric excitation mechanism. However, the ellipsoidal vibration mode can be excited in slightly elongated particles [9], where the spherical symmetry is broken.

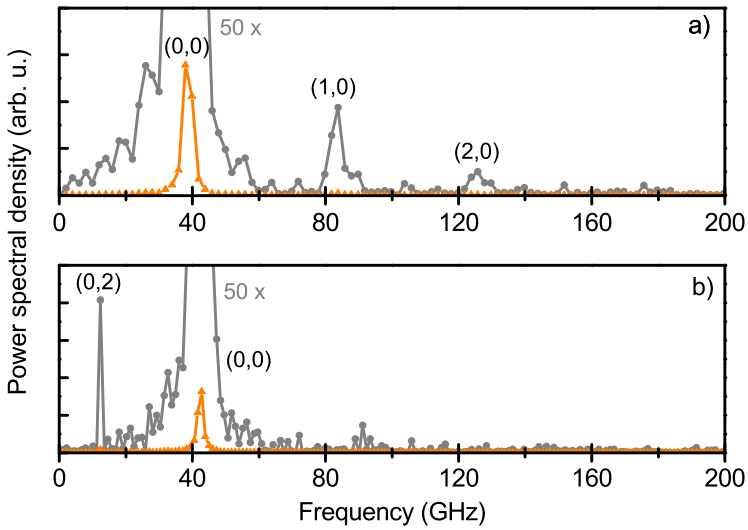

Figure S2 Vibration modes of single 80 nm gold spheres optically trapped in water. Vibrational spectra are dominated by the fundamental breathing mode $\Omega_{0,0}$ around 40 GHz, but weak traces of other vibrational modes are detected. (a) Vibrational spectrum of a sphere with a breathing mode at $\Omega_{0,0} = 38.8\,\mathrm{GHz}$. Weak traces of the higher order radial modes $(n, l) = (1, 0)$ at $\Omega_{1,0}$ (84 GHz, $2.16 \times \Omega_{0,0}$) and $(n, l) = (2, 0)$ at $\Omega_{2,0}$ (126 GHz, $3.25 \times \Omega_{0,0}$) are detected. (b) Vibrational spectrum of a sphere with a breathing mode at $\Omega_{2,0} = 42.4\,\mathrm{GHz}$. An additional vibration mode at 12.5 GHz ($0.29 \times \Omega_{0,0}$) is attributed to the $(0, 2)$ ellipsoidal deformation mode.

Vibrations of an embedded spherical particle

We calculate frequencies and damping times of the breathing mode of an elastic gold sphere embedded in an elastic medium, according to the complex frequency model [10, 11], for several matrix materials, see table S 4.

For a gold sphere in water, we estimate the effect of viscous damping following the approach by Saviot *et al.*, that calculates the effective (complex) velocities of sound [12] in the liquid. We find a minor correction upon inclusion of viscous damping. Both bulk viscosity and shear viscosity contribute to the damping of sound waves. The shear viscosity -also known as dynamic viscosity- is the more commonly used viscosity, governing for example the diffusion constants appearing in the Brownian motion of particles in liquid. The bulk viscosity -also known as volume viscosity or second viscosity coefficient- needs to be taken into account when compressibility of the liquid cannot be neglected, as is the case for sound waves [13].

Note that for the calculation of the viscous damping, viscosity values were taken for water at 30 °C, as in Saviot *et al.* [12]. We estimate that the temperature of the trapped particles is significantly higher, and is in the range 80-100 °C for the trapping powers used in our experiment, see Table S 2. However, the damping times calculated for non-viscous water and viscous water at 30 °C form upper and lower bounds to the damping time in the experiment, respectively. This is because both shear and bulk viscosity decrease with increasing temperature. At higher temperatures the effect of viscous damping on the nanoparticle vibration is thus reduced.

In the calculation of the viscous damping we have used the viscosity values of water at at 30 °C because we could not find measurements of the bulk viscosity in the temperature range 80-100 °C. For the commonly used shear viscosity accurate measurements on water are available in the whole range from the melting point to the critical point, see for example the NIST chemistry webbook [14]. The temperature dependence of the shear viscosity is well described by an exponential decay with temperature, an empirical relation known as the Vogel-Fulcher law [15]. For the bulk viscosity only a few experimental studies are available [16, 13, 17], for temperatures up to 50 °C [17]. In the temperature range 7-50 °C, the bulk viscosity decreases monotonically with temperature, closely following an exponential decay [17].

The effect of viscosity on the damping of the breathing mode of the nanoparticle is small, and our results are insensitive to the details of the calculation. For the results in the main text, we have made the arbitrary choice to use the damping times calculated for viscous water at 30 °C.

Matrix	ρ(kg/m^3)	v_L (m/s)	v_T (m/s)	T (ps)	τ (ps)	Q
BK7 glass	2240	5100	2840	25.9	77.8	9.44
Polystyrene	1300	2350	2000	26.1	236	28.4
Water (non-viscous)	1000	1500	-	26.4	453	54.0
Water (viscous, 30 °C)	1000	$1521 + 254i$	$322 + 322i$	26.4	443	52.5
Gold	19700	3240	1200	-	-	-

Table S4 Calculated frequencies, damping times and quality factors of the fundamental breathing mode of a 80 nm gold sphere embedded in several matrices.

Ratio of breathing and extension mode frequency of gold nanorods

Figure S 3 displays the scaling of the breathing mode frequency ν_{br} to the extensional mode frequency ν_{ext} measured on single gold nanorods in an optical trap in water. Data on the same nanorods is reported in Fig. 3 from the main text. In addition to the data on the 7 PEG-coated rods from the main text, data on 2 nanorods stabilized in CTAB are included.

It is expected that the frequency ratio $\nu_{\mathrm{br}}/\nu_{\mathrm{ext}}$ is proportional to the aspect ratio of the rod [18]. In our experiment we can estimate the aspect ratio for each individual nanorod in the trap from the longitudinal plasmon resonance λ_{L}, obtained from the rods scattering spectrum. Here, we approximate AR $= (\lambda_{\mathrm{L}} - 410)/85$, with λ_{L} in units of nm, by calculation of the plasmon resonance of a gold ellipsoidal particle in water, in the dipole limit. The data points in Figure S 3 all fall on a horizontal line, indicating that the frequency ratio $\nu_{\mathrm{br}}/\nu_{\mathrm{ext}}$ is strongly correlated to the rods aspect ratio. The graph also displays the theoretical values calculated for a polycrystalline rod [18] (dashed line, $\nu_{\mathrm{br}}/\nu_{\mathrm{ext}} = 2.32 \times$ AR) and for a single-crystalline rod with its long axis along the [1 0 0] direction (dotted line, $\nu_{\mathrm{br}}/\nu_{\mathrm{ext}} = 3.24 \times$ AR) [19]. It appears that the data are closer to the value expected for polycrystalline rods than for a single crystal rod. However, this attribution depends critically on the absolute value of the aspect ratio. It is difficult to obtain an accurate absolute relation between the aspect ratio of the rod and its longitudinal plasmon resonance. Calculated values of the resonance depend sensitively on the exact shape of the tip of the rod, and on the exact thickness and structure of the capping layer, parameters that are not known with high precision for the individual rods in our experiment. Therefore, we do yet draw quantitative conclusions from the absolute value of the proportionality constant found in Fig. S 3. The assumption of a linear relation between aspect ratio and plasmon resonance is more robust, as indicated by our data.

To come to a quantitative conclusion about the scaling of vibration mode frequencies in gold nanorods, it would be necessary to determine the exact aspect ratio of each individual nanorod in the trap by electron microscopy on the nanorod, as was done previously for nanorods immobilized on a substrate [19].

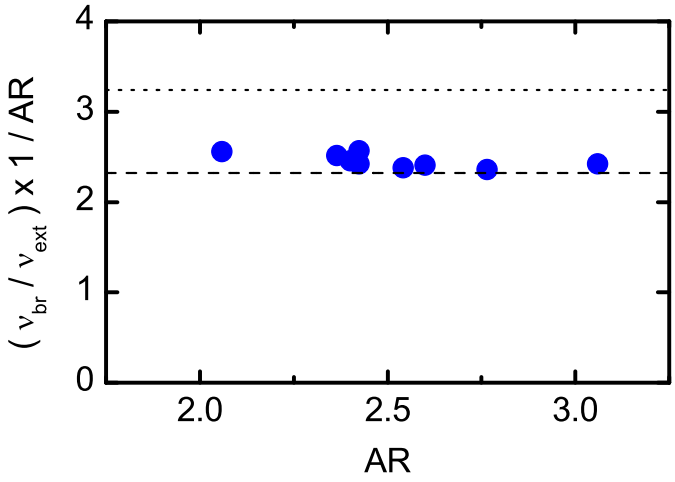

Figure S3 Ratio of breathing mode and extensional mode frequencies of optically trapped nanorods, as function of aspect ratio. The aspect ratio was deduced from the measured wavelength of the longitudinal plasmon resonance λ_R via AR $= (\lambda_R - 410)/85$, with λ_R in nm. Dashed line: theoretical value for a gold nanorod with polycrystalline elastic constants [18, 19]. Dotted line: theoretical value for a single crystalline rod, with the long axis of the rod in the the [1 0 0] direction.

References

[1] P. V. Ruijgrok, N. R. Verhart, P. Zijlstra, A. L. Tchebotareva, and M. Orrit, "Brownian fluctuations and heating of an optically aligned gold nanorod," Phys. Rev. Lett. **107**, 037401 (2011).

[2] P. B. Johnson and R. W. Christy, "Optical constants of the noble metals," Phys. Rev. B **6**, 4370–4379 (1972).

[3] C. F. Bohren and D. R. Huffman, *Absorption and Scattering of Light by Small Particles* (Wiley, 1998).

[4] C. Novo, D. Gomez, J. Pérez-Juste, Z. Zhang, H. Petrova, M. Reismann, P. Mulvaney, and G. V. Hartland, "Contributions from radiation damping and surface scattering to the linewidth of the longitudinal plasmon band of gold nanorods: a single particle study," Phys. Chem. Chem. Phys. **8**, 3540–3546 (2006).

[5] H. Petrova, J. Perez Juste, I. Pastoriza-Santos, G. V. Hartland, L. M. Liz-Marzán, and P. Mulvaney, "On the temperature stability of gold nanorods: comparison between thermal and ultrafast laser-induced heating," Phys. Chem. Chem. Phys. **8**, 814–821 (2006).

[6] P. Zijlstra, J. W. M. Chon, and M. Gu, "White light scattering spectroscopy and electron microscopy of laser induced melting in single gold nanorods," Phys. Chem. Chem. Phys. **11**, 5915–5921 (2009).

[7] H. Lamb, "On the vibrations of an elastic sphere," Proc. Lon. Mat. Soc. **13**, 189–212 (1882).

[8] L. Saviot, B. Champagnon, E. Duval, I. A. Kudriavtsev, and A. I. Ekimov, "Size dependence of acoustic and optical vibrational modes of CdSe nanocrystals in glasses," J. Non-Cryst. Solids **197**, 238–246 (1996).

[9] A. L. Tchebotareva, M. A. van Dijk, P. V. Ruijgrok, V. Fokkema, M. H. S. Hesselberth, and M. Orrit, "Acoustic and optical modes of single dumbbells of gold nanoparticles," ChemPhysChem **10**, 114–114 (2009).

[10] V. A. Dubrovskiy and V. S. Morochnik, "Natural vibrations of a spherical inhomogeneity in an elastic medium," Izv. Earth Phys. **17**, 494–504 (1981).

[11] C. Voisin, D. Christofilos, N. Del Fatti, and F. Vallée, "Environment effect on the acoustic vibration of metal nanoparticles," Physica B **316**, 89–94 (2002).

[12] L. Saviot, C. H. Netting, and D. B. Murray, "Damping by bulk and shear viscosity of confined acoustic phonons for nanostructures in aqueous solution," J. Phys. Chem. B **111**, 7457–7461 (2007).

[13] A. S. Dukhin and P. J. Goetz, "Bulk viscosity and compressibility measurement using acoustic spectroscopy," J. Chem. Phys. **130**, 124519 (2009).

[14] NIST, "Nist chemistry webbook," Http://webbook.nist.gov/chemistry/fluid/.

[15] D. Rings, R. Schachoff, M. Selmke, F. Cichos, and K. Kroy, "Hot brownian motion," Phys. Rev. Lett. **105**, 090604 (2010).

[16] U. S. Litovitz and E. H. Carnevale, "Effect of pressure on sound propagation in water," J. App. Phys. **26**, 816–820 (1955).

[17] M. J. Holmes, N. G. Parker, and M. J. Povey, "Temperature dependence of bulk viscosity in water using acoustic spectroscopy," J. Phys.: Conf. Ser. **269**, 012011 (2011).

[18] M. Hu, X. Wang, G. V. Hartland, P. Mulvaney, J. Pérez Juste, and J. E. Sader, "Vibrational response of nanorods to ultrafast laser induced heating: Theoretical and experimental analysis," J. Am. Chem. Soc. **125**, 14925–14933 (2003).

[19] P. Zijlstra, A. L. Tchebotareva, J. W. M. Chon, M. Gu, and M. Orrit, "Acoustic oscillations and elastic moduli of single gold nanorods," Nano Lett. **8**, 3493–3497 (2008).